MDPI

Article

A Comparative Study of Machining Property in Inconel 718 Superalloy Grinding with Al_2O_3- and CBN/Fe-Based Spherical Magnetic Abrasives

Linzhi Jiang, Guixiang Zhang *, Haozhe Zhang, Yandan Xia and Jinli Xiang

School of Mechanical Engineering, Shandong University of Technology, Zibo 255000, China
* Correspondence: zhanggx2013@163.com

Abstract: A comparative analysis was studied on the finishing performance of spherical CBN/Fe-based magnetic abrasive particles (MAPs) and Al_2O_3/Fe-based magnetic abrasive particles (MAPs) prepared by the gas atomization method in the magnetic abrasive finishing (MAF) of the Inconel 718 superalloy. In the MAF, it was found that compared with Al_2O_3/Fe-based MAPs, CBN/Fe-based MAPs have a lower grinding temperature and generate less heat during the grinding of the Inconel 718 superalloy. The grinding pressure generated on the workpiece is relatively stable (Al_2O_3/Fe-based MAPs have a larger fluctuation range of grinding pressure on the workpiece surface during the grinding process). The surface roughness of the workpiece rapidly drops from Ra 0.57 μm to Ra 0.039 μm, and the material removal reaches 42 mg within 20 min. After finishing, the scratches on the surface of the workpiece basically disappear, the contour curve is relatively flat, and there is almost no adhesion on the surface of the workpiece. The mirror effect of the superalloy surface is good, and ultimately a better surface quality can be obtained.

Keywords: magnetic abrasive finishing; Inconel 718 superalloy; spherical CBN- and Al_2O_3/Fe-based magnetic abrasive particles; finishing performance

1. Introduction

Due to the high hardness, strength, viscosity, and toughness of the Inconel 718 superalloy, it is difficult to meet the required quality requirements using traditional grinding techniques [1–3]. Therefore, magnetic abrasive finishing (MAF) technology is used to attempt to improve its surface quality [4–7].

As a machining tool for MAF, the performance of magnetic abrasive particles (MAPs) plays a crucial role in the grinding process [8–11]. Mohammad et al. used Al_2O_3 MAPs prepared by the sintering method and simulated the surface polishing of silicon wafers with the MAF process by a SPH/FEM coupled algorithm [12]. Guo et al. used MAPs mixed with Al_2O_3 grains and iron powders for the local vibration-assisted MAF of rectangular microfeatures. The workpiece surface quality was improved, and the form of microfeatures was well maintained [13]. Heng et al. studied three magnetic pole designs that affect the surface quality and roundness precision of ZrO_2 bars by using unbonded MAPs mixed with iron particles, diamond compound paste, carbon nanotubes, and light oil [14]. Atul et al. investigated the optimization of MAF taking into account the material removal rate and surface characteristics using a hybrid nature-inspired algorithm. The processing tool used in the experiment was MAPs mixed with iron and boron carbide powders prepared by the sintering method [15]. The advantage of MAF over other grinding methods is that MAPs have good fluidity and adaptability, which can effectively grind complex parts and surfaces [16,17]. Therefore, the ideal MAP model should be spherical, and the distribution of ceramic abrasive particles on the surface of the iron matrix should be uniform and dense (Figure 1) [18].
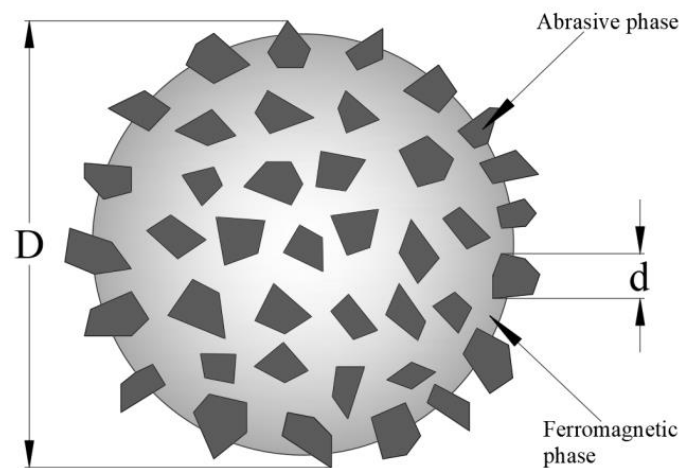
Figure 1. Ideal model of MAPs.

We have successfully prepared Al_2O_3, SiC, and CBN/Fe-based spherical MAPs using the gas atomization method, which is very close to the ideal MAP model [19–21]. In order to study the processing performance of MAPs prepared by the atomization method and further improve the surface quality of the Inconel 718 superalloy, Al_2O_3- and CBN/Fe-based spherical MAPs were used for the MAF of an Inconel 718 superalloy workpiece. The changes in surface morphology, roughness, and material removal before and after processing were compared. The grinding temperature and pressure changes of the two types of MAPs on the superalloy workpiece were studied, and the main reasons for the different processing performance of the two types of MAPs before and after grinding were observed and analyzed.

2. Materials and Methods

2.1. Experimental Principles

Magnetic abrasive finishing technology is an advanced finishing method that combines magnetic fields and magnetic abrasive particles to apply to complex surfaces and small parts of various difficult-to-machine materials. During the finishing process, the MAPs that are adsorbed and flowing by a magnetic field generate relative motion with the surface of the part. The sharp ceramic abrasive particles on the surface of the MAPs perform micro-cutting relative to the surface of the part, thereby achieving ultra-precision finishing. The schematic diagram of MAF is shown in Figure 2.
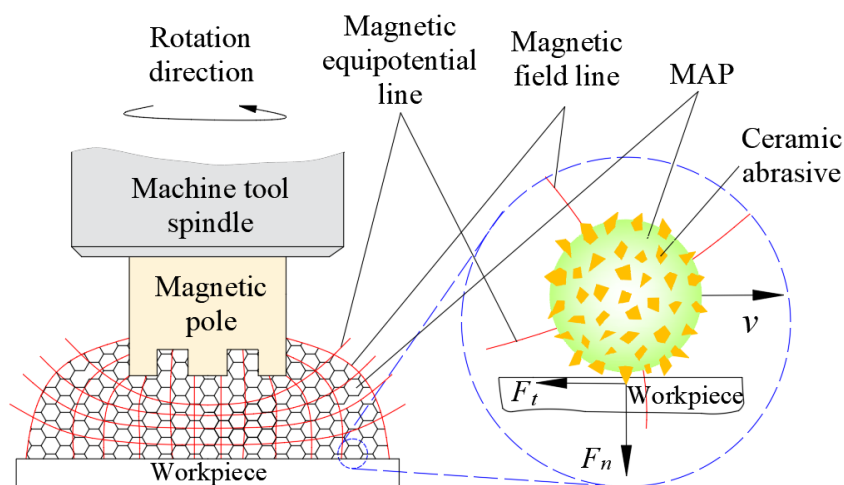
Figure 2. Schematic diagram of magnetic abrasive finishing.

2.2. Experimental Materials

The MAPs used in the experiment are Al_2O_3- (Figure 3a) and CBN/Fe-based (Figure 3b) spherical MAPs prepared by the gas atomization method. The mechanical properties between Al_2O_3 and CBN are shown in Table 1. Figure 4 presents a schematic diagram of the ceramic/Fe-based spherical MAP preparation system. First, the ceramic abrasives are added to the mixing device. The iron matrix material is added into the melting furnace and heated to 1650 °C. Then, the molten iron matrix is poured into the heat crucible, while the mixing device is opened at the same time. The falling metal flow is blown and atomized into ceramic/Fe-based composite droplets by N_2 mixed with ceramic abrasives sprayed from the atomizing nozzle. Finally, the composite droplets are cooled and solidified during the falling process to form spherical MAPs. It can be seen that the MAPs have good sphericity, and the Al_2O_3 and CBN ceramic abrasive phases are uniformly and densely distributed on the surface of the iron matrix, which is basically consistent with the ideal MAP model. The workpiece being processed is the Inconel 718 superalloy, with dimensions of $60 \times 30 \times 2$ mm and an initial roughness of 0.57 μm.
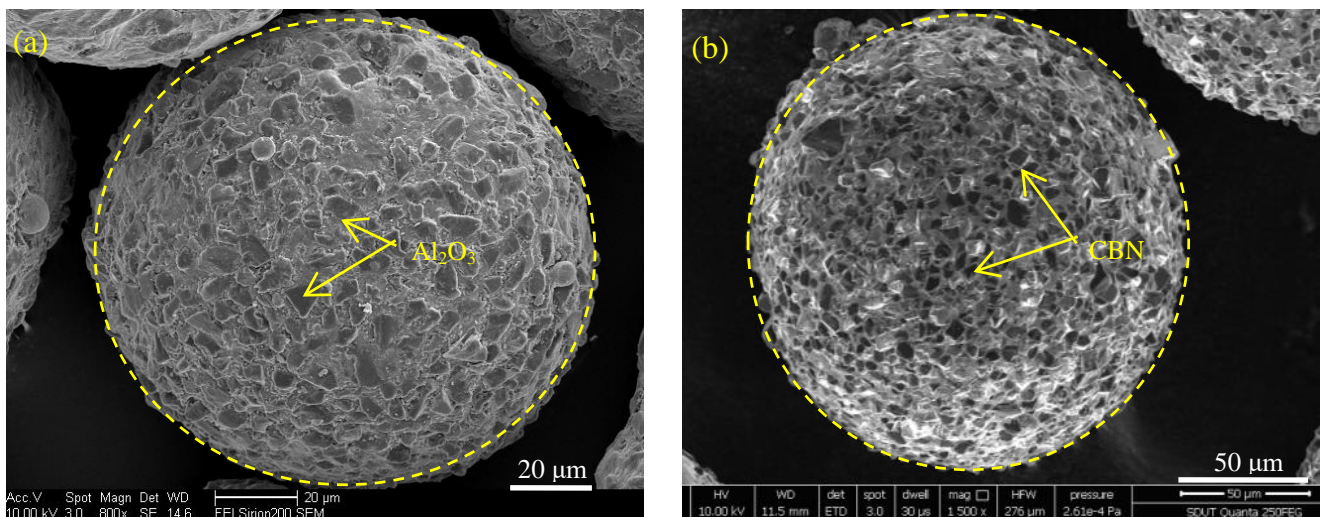
Figure 3. (**a**) Al_2O_3- and (**b**) CBN/Fe-based spherical MAPs prepared by gas atomization.

Table 1. Mechanical properties between Al_2O_3 and CBN.

Material	Al_2O_3	CBN
Density/g·cm^{-3}	3.5	3.48
Nup hardness/N·mm^{-2}	21,000~24,000	45,000~48,000
Bending strength/N·mm^{-2}	80~90	300
Compressive strength/N·mm^{-2}	3000	7200
Coefficient of thermal expansion/10^{-6}·K^{-1}	8.5	2.5~2.6
Thermal diffusivity/m^2·s^{-1}	0.36	4.03
Melting point/°C	2050	2220
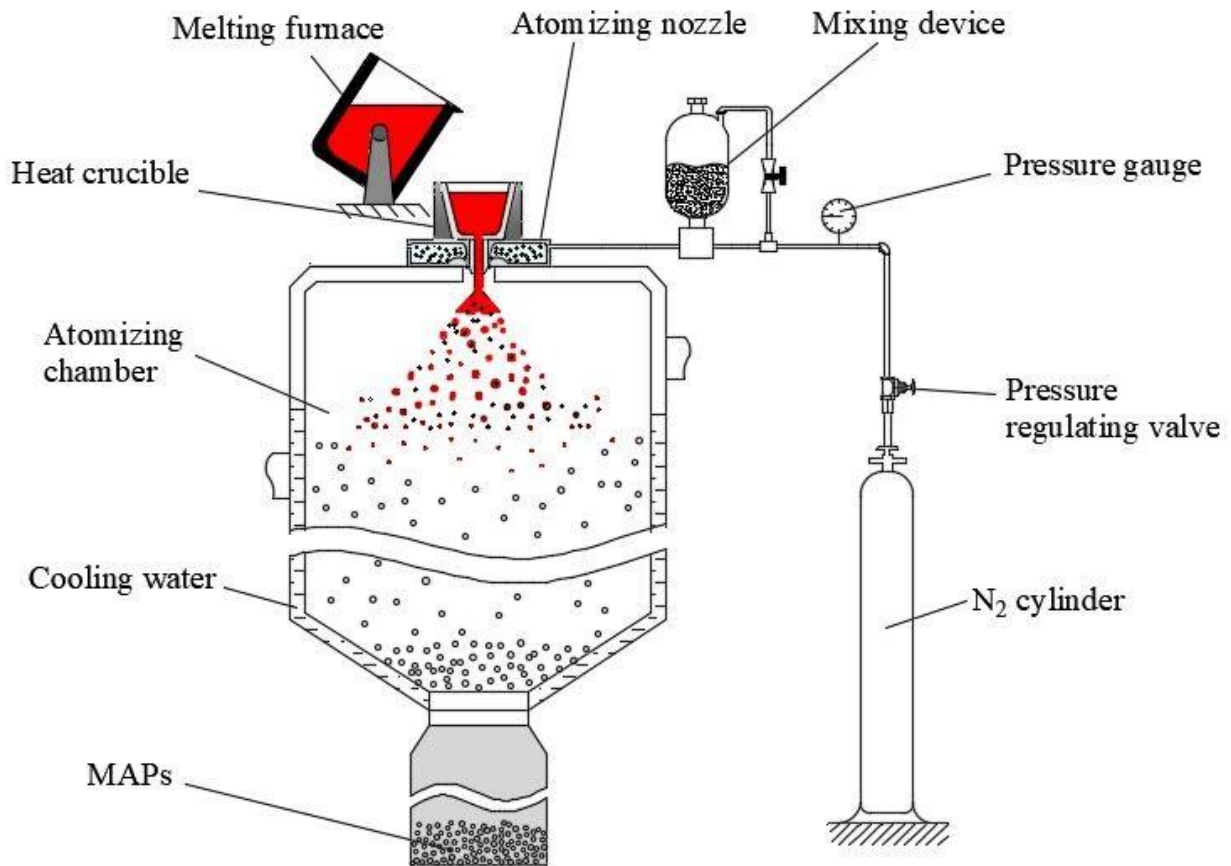
Figure 4. Schematic diagram of ceramic/metal spherical MAP preparation system.

2.3. Experimental Setup and Conditions

The MAF device is an XK7136C CNC milling machine, and its spindle part has been designed and improved. The milling cutter on the original milling machine spindle was replaced with a self-designed and developed slotted magnetic pole, which was installed on the machine spindle through a sleeve. Adjustable fixtures were installed below the spindle for the easy clamping and grinding of workpieces of different shapes and sizes (Figure 5).
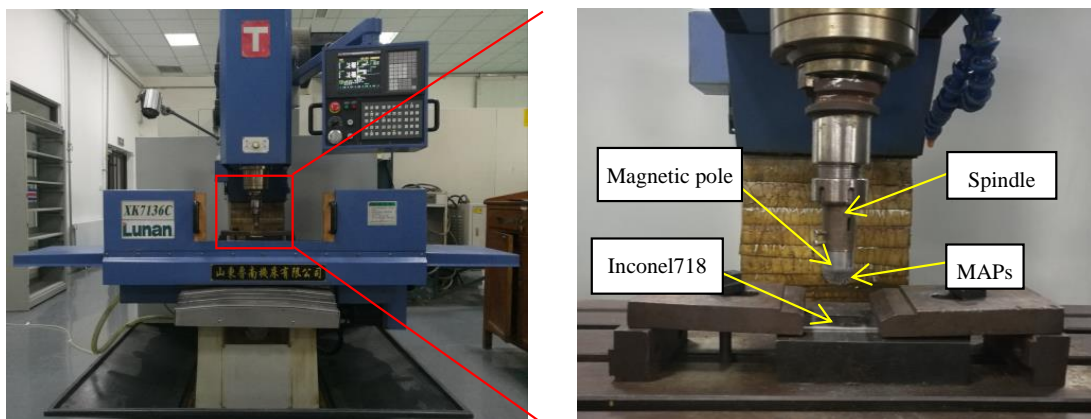
Figure 5. Experimental setup of MAF.

A comparative analysis was performed of MAF on the surface of the Inconel 718 superalloy workpiece using Al_2O_3- and CBN/Fe-based spherical MAPs under the same experimental conditions. The experimental parameters are shown in Table 2.

Table 2. MAF experiment parameters.

Processing Parameter	Value
Workpiece	Inconel 718 superalloy ($60 \times 30 \times 2$ mm)
MAPs	Al_2O_3- and CBN/Fe-based spherical MAPs
Amount of MAPs	2 g
Spindle speed	1200 r/min
Feed rate	15 mm/min
Working gap	2 mm
Processing time	30 min

During the experiment, a handheld roughness meter and a precision electronic balance were used to accurately measure the surface roughness value and material removal amount of the workpiece. A depth-of-field microscope and a white-light interferometer were used to observe the two-dimensional and three-dimensional surface morphology changes of the workpiece before and after grinding. A temperature tester was used to measure and analyze the surface temperature changes of the workpiece. A pressure tester was used to detect the changes in grinding pressure on the surface of the workpiece.

3. Results and Discussion

3.1. Surface Morphology Changes of Inconel 718 Superalloy

The comparison of the two-dimensional and three-dimensional morphology of the Al_2O_3- and CBN/Fe-based spherical MAPs prepared by gas atomization on the surface of the Inconel 718 superalloy workpiece before and after grinding is shown in Figure 6.
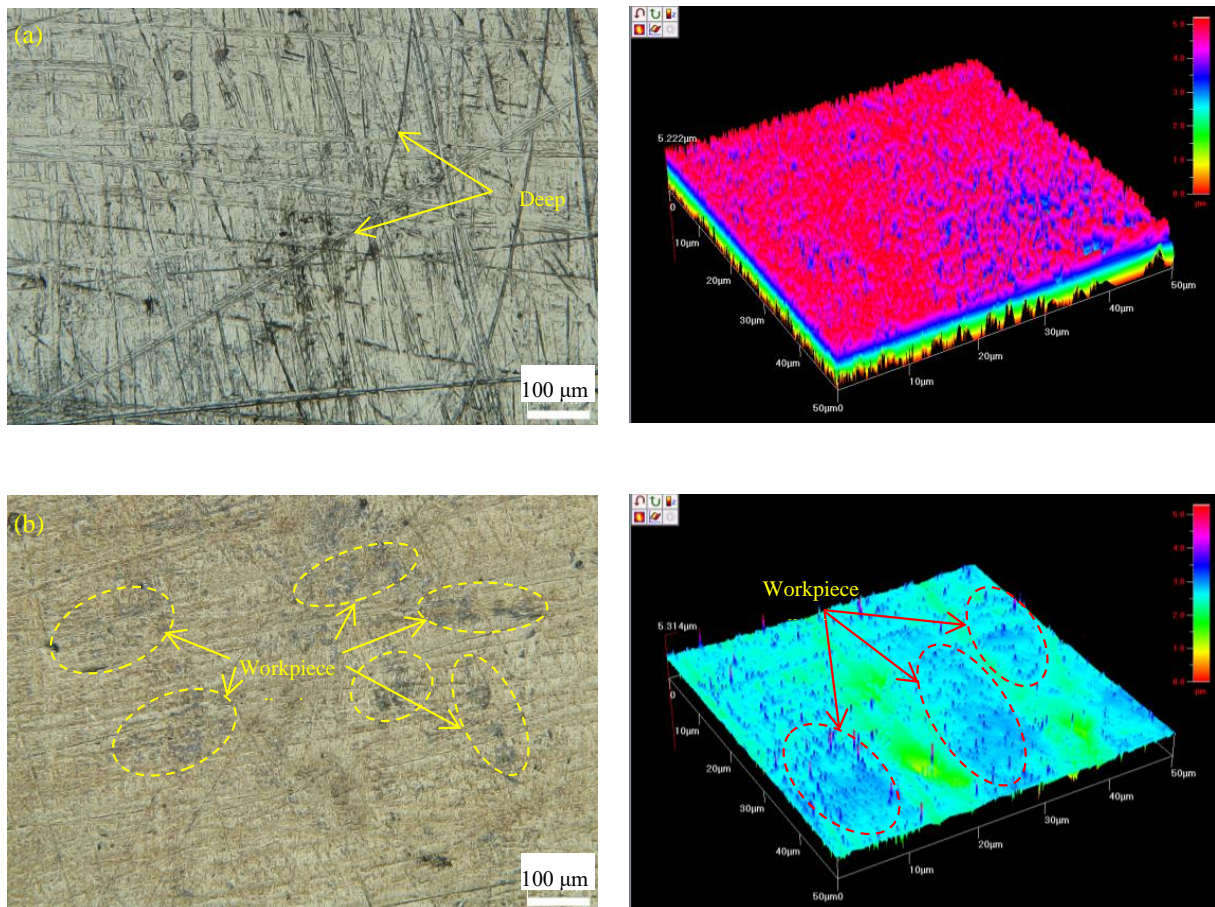
Figure 6. *Cont*.
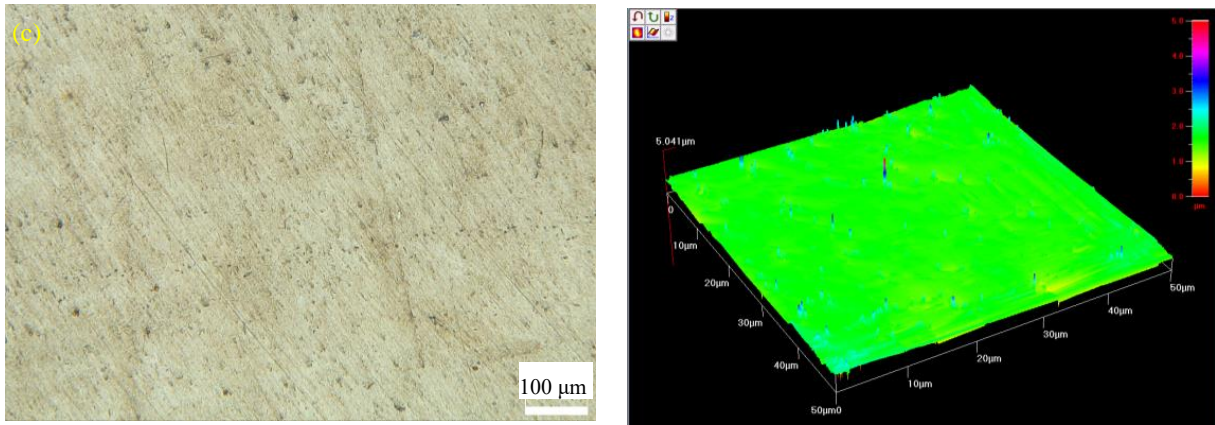
Figure 6. Morphology of Inconel 718 alloy surface before and after MAF with two types of MAPs: (**a**) original, (**b**) Al_2O_3 MAPs, (**c**) CBN MAPs.

It can be seen that there are numerous scratches on the surface of the workpiece before grinding, with varying depths and poor surface quality (Figure 6a). After being ground with the Al_2O_3/Fe-based MAPs, the surface scratches of the Inconel 718 superalloy workpiece become significantly shallower, and the surface quality is improved. However, there are some adherents attached to the workpiece surface (Figure 6b). After being ground with the CBN/Fe-based MAPs, the surface scratches of the workpiece have basically disappeared, and the surface quality is significantly improved. Moreover, there is almost no adhesion on the surface of the workpiece (Figure 6c).

The comparison of the surface profile curves and mirror effects of the two types of MAPs on the surface of the Inconel 718 superalloy workpiece before and after grinding is shown in Figure 7.
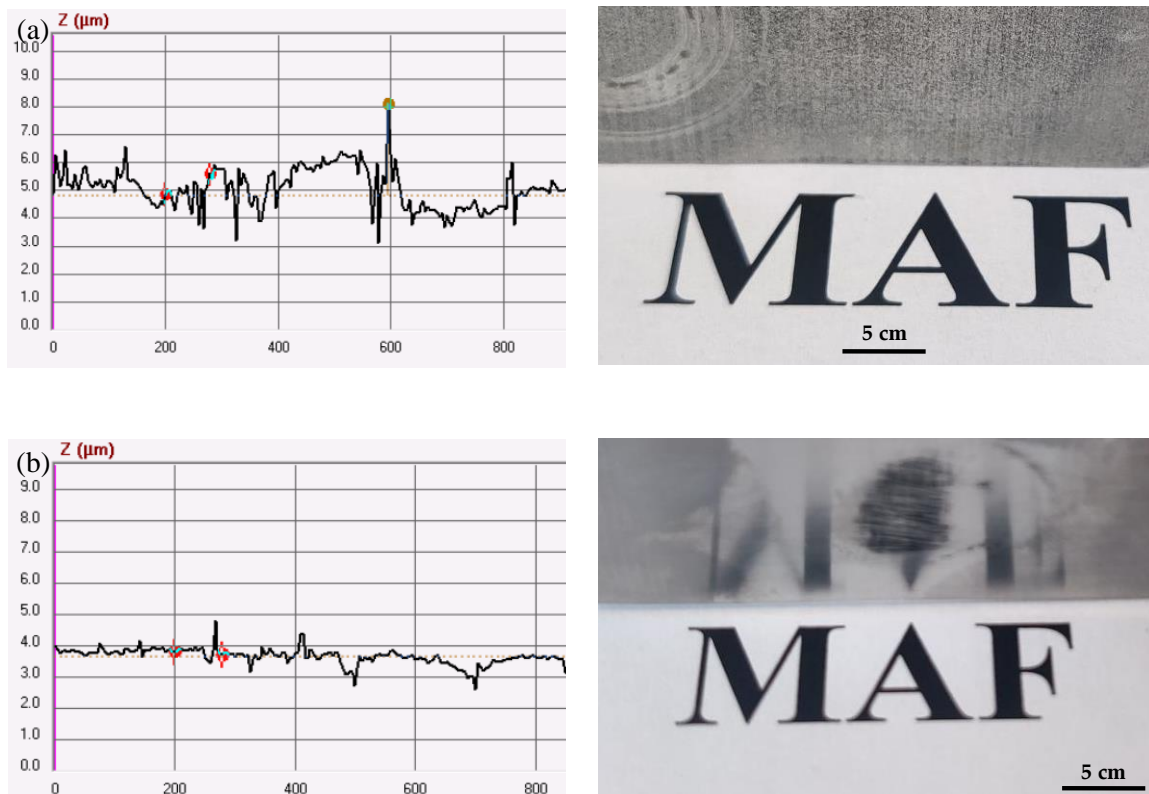
Figure 7. *Cont.*
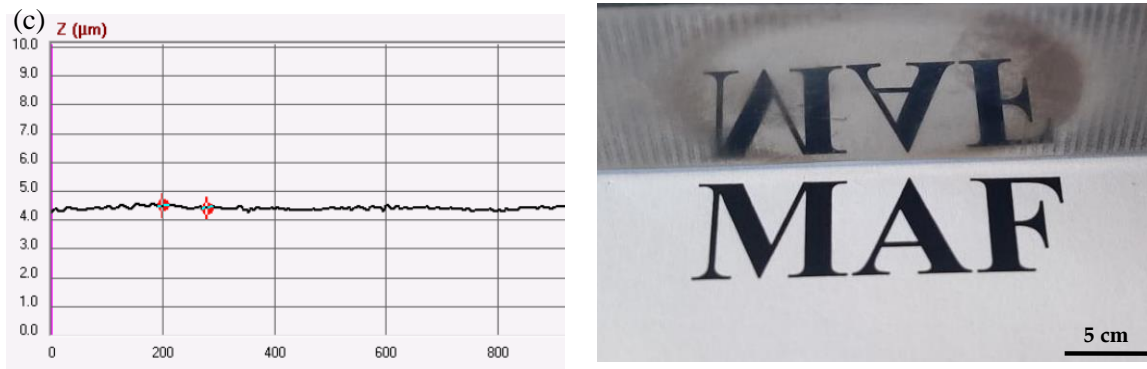
Figure 7. Profile curves and mirror effects of Inconel 718 alloy surface before and after MAF with two types of MAPs: (**a**) original, (**b**) Al_2O_3 MAPs, (**c**) CBN MAPs.

It can be seen that the fluctuation of the surface contour curve of the Inconel 718 super-alloy workpiece after grinding with Al_2O_3/Fe-based MAPs slowed down, and the mirror effect is relatively blurry (Figure 7b). At the same time, there is a large amount of adhesive residue on the surface of the workpiece. After grinding with the CBN/Fe-based MAPs, the surface contour curve of the superalloy is relatively flat, and the word "MAF" in the mirror effect is relatively clear. There is almost no adhesive residue on the surface of the workpiece (Figure 7c). This indicates that CBN/Fe-based MAPs have better grinding performance than Al_2O_3/Fe-based MAPs in the MAF of the Inconel 718 superalloy workpiece.

3.2. Changes in Surface Roughness and Material Removal of Inconel 718 Superalloy

Two types of MAPs were used to grind the surface of the Inconel 718 superalloy workpiece, and the surface roughness and material removal of the workpiece were tested every 5 min. The changes in surface roughness and material removal of the workpiece are shown in Figure 8.
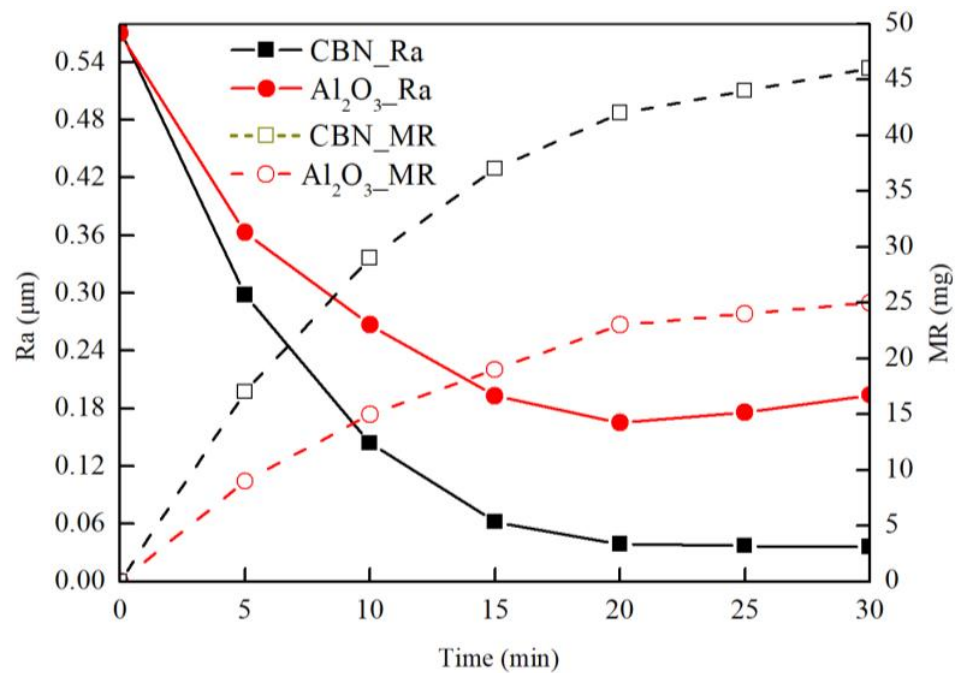
Figure 8. Comparison of surface roughness and material removal of Inconel 718 superalloy ground with two types of MAPs.

It can be seen that the surface roughness of the workpiece decreases significantly during the grinding process of the Inconel 718 superalloy with the CBN/Fe-based MAPs. Within 20 min, the initial roughness Ra decreases rapidly from 0.57 μm to 0.039 μm, the material removal amount reaches 42 mg within 20 min, and then the value stabilizes without significant changes. When the Inconel 718 superalloy workpiece is ground by Al_2O_3/Fe-based MAPs, the surface roughness Ra of the workpiece decreases to 0.165 μm, the material removal amount reaches 23 mg within 20 min, and the surface roughness of the workpiece shows an upward trend with continued grinding. This is because compared with CBN/Fe-based MAPs, Al_2O_3/Fe-based MAPs are more prone to adhesion with the surface of the Inconel 718 superalloy workpiece. When the grinding time is longer, not only does the processing performance of Al_2O_3/Fe-based MAPs deteriorate, but the surface of the superalloy is also prone to adhesion of MAPs, which in turn leads to a decrease in the surface quality and an increase in the surface roughness of the workpiece.

3.3. Surface Temperature Changes of Inconel 718 Superalloy

The highest temperature generated during the grinding of the Inconel 718 superalloy with two types of MAPs is shown in Figure 9. It can be seen that the highest temperature on the surface of the workpiece generated by the CBN/Fe-based MAPs is 38.0 °C (Figure 9a), while the highest temperature generated by the Al_2O_3/Fe-based MAPs is 62.2 °C (Figure 9b).
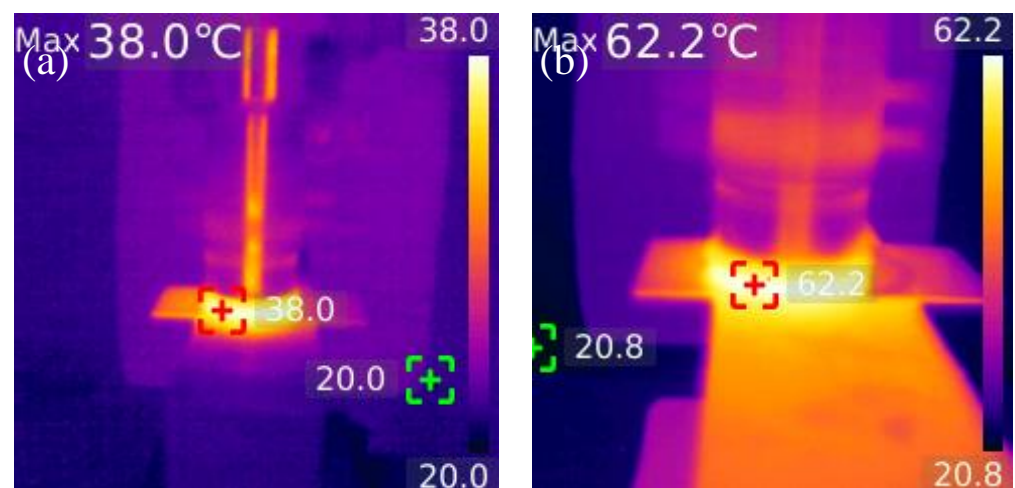
Figure 9. The highest temperature generated by grinding Inconel 718 superalloy with (**a**) CBN- and (**b**) Al_2O_3/Fe-based spherical MAPs.

Compared with CBN/Fe-based MAPs, Al_2O_3/Fe-based MAPs generate more heat during the grinding process. This is because the thermal conductivity of the Al_2O_3 ceramic abrasive phase is relatively low, and the thermal conductivity value rapidly decreases with the increase in temperature, while the thermal conductivity of the CBN ceramic abrasive phase is much higher than that of Al_2O_3 ceramic, and its thermal conductivity value remains basically unchanged with the change in temperature. Therefore, as the temperature increases, Al_2O_3/Fe-based MAPs will generate more heat in MAF. Meanwhile, the hardness of the CBN ceramic abrasive phase is much higher than that of the Al_2O_3 ceramic abrasive phase, and it is sharper than the Al_2O_3 ceramic. Under the same conditions, the grinding force of the CBN ceramic abrasive on the surface of the Inconel 718 superalloy is smaller, and the grinding heat generated by friction is less.

The surface temperature changes of the workpiece during the grinding of the Inconel 718 superalloy with two types of MAPs are shown in Figure 10.
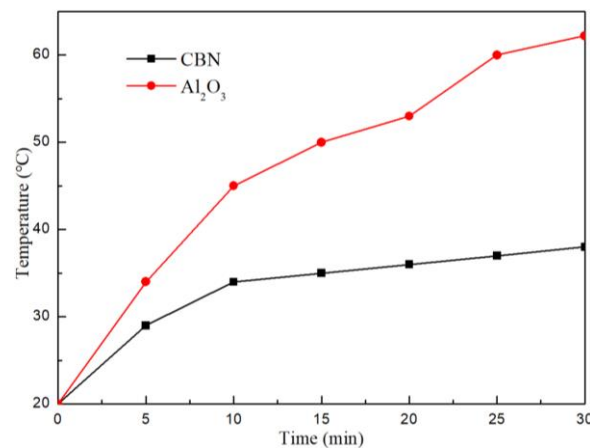
Figure 10. Surface temperature changes of Inconel 718 superalloy ground with two types of MAPs.

It can be seen that when CBN/Fe-based MAPs are used to grind the Inconel 718 superalloy, the temperature rises from 20 °C to 34 °C within 10 min, and there is no significant change in temperature during the subsequent processing time. The grinding temperature generated by the Al_2O_3/Fe-based MAPs during the grinding process continuously increases with the increase in processing time. This is because the thermal stability of the CBN ceramic abrasive is much better than that of Al_2O_3 ceramic abrasive, and its thermal conductivity remains excellent with temperature changes during the grinding process. At the same time, the hardness of the CBN ceramic abrasive is higher than that of the Al_2O_3 ceramic abrasive, and its wear resistance is better. Even in the later stage of grinding, their sharpness can still be maintained, so the temperature tends to stabilize in the later stage of grinding. However, the thermal conductivity of Al_2O_3/Fe-based MAPs rapidly deteriorates with the increase in temperature during the grinding process. The wear of the Al_2O_3 ceramic abrasive intensifies, and the adhesion phenomenon with the alloy surface intensifies, resulting in a continuous increase in grinding temperature.

3.4. Surface Grinding Force Changes of Inconel 718 Superalloy

The variation in grinding force on the workpiece surface during the grinding of the Inconel 718 superalloy with two types of MAPs is shown in Figure 11. It can be seen that the grinding force generated by the CBN/Fe-based MAPs on the surface of the workpiece is relatively stable, and the change in grinding force is not significant in MAF. After 30 min of grinding, the grinding force increases from 5 N to 6.5 N. However, the grinding force generated by the Al_2O_3/Fe-based MAPs on the surface of the workpiece fluctuates greatly, and the grinding force increases rapidly. Within 30 min, the grinding force increases from 5 N to 8.8 N.
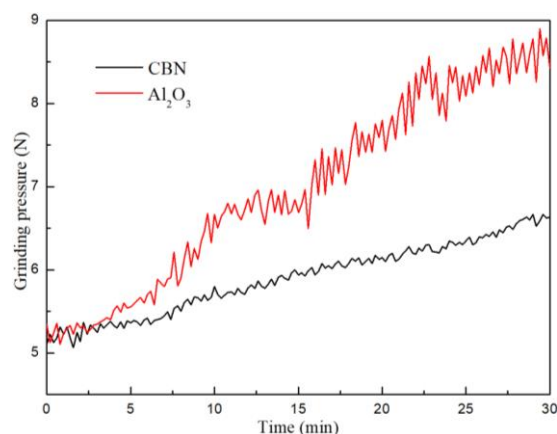
Figure 11. Grinding force changes of Inconel 718 superalloy ground with two types of MAPs.

This is because the CBN ceramic abrasive has higher hardness, better wear resistance and sharpness, and generate less grinding force during the grinding process. The grinding force increases slowly with the change in processing time. On the other hand, Al_2O_3/Fe-based MAPs are more prone to adhesion with the surface of the Inconel 718 superalloy, resulting in an increasing amount of adhesion between the two and an increasing grinding force on the workpiece surface. At the same time, due to the influence of the adhesion material, the grinding performance of the Al_2O_3/Fe-based MAPs is no longer stable, and the superalloy surface becomes uneven due to the adhesion material, resulting in significant fluctuations in the grinding force. When the CBN/Fe-based MAPs are used to grind the Inconel 718 superalloy, the processing stability is good, and there is very little adhesion with the workpiece, so the fluctuation of the grinding force formed is not significant.

4. Conclusions

When the magnetic abrasive finishing method is used to grind the Inconel 718 superalloy, the surface roughness of the alloy can be reduced to Ra 0.039 μm, which is much higher than the surface quality achieved by traditional grinding methods. Although Al_2O_3/Fe-based MAPs have a certain grinding effect when grinding the Inconel 718 superalloy, the processing effect is still far less significant than the CBN/Fe-based MAPs. This is because the Inconel 718 superalloy has good high-temperature strength and high plasticity, so the grinding force generated by MAPs on its surface is much greater than that of ordinary materials. At the same time, the Inconel 718 superalloy has a low thermal conductivity, only one-third to one-fifth of ordinary steel workpieces. Therefore, when using ordinary-hardness and poor-thermal-conductivity MAPs such as Al_2O_3/Fe-based MAPs to grind the Inconel 718 superalloy, the grinding force generated by the MAPs on the surface of the workpiece is greater, the grinding temperature is higher, and adhesion phenomenon is prone to occur between the MAPs and workpiece, thereby affecting the processing performance of the MAPs. Therefore, CBN/Fe-based MAPs with higher hardness and better thermal conductivity are more suitable for grinding difficult-to-machine materials such as the Inconel 718 superalloy, thus meeting the high-quality requirements of the workpiece surface.

Author Contributions: L.J. contributed to the investigation, conduction of MAF experiments and writing of the original draft, writing of the review, and editing. G.Z. contributed to the writing of the review, editing, and funding acquisition. H.Z., Y.X. and J.X. contributed to the review and editing with the order provided. All authors have read and agreed to the published version of the manuscript.

Institutional Review Board Statement: Not applicable.

Informed Consent Statement: Not applicable.

Data Availability Statement: Data are contained within this article.

Conflicts of Interest: The authors declare no conflicts of interest.

References

1. Sebbe, N.P.V.; Fernandes, F.; Silva, F.J.G.; Pedroso, A.F.V.; Sales-Contini, R.C.M.; Barbosa, M.L.S.; Durão, L.M.; Magalhães, L.L. Wear Behavior of TiAlVN-Coated Tools in Milling Operations of INCONEL® 718. *Coatings* **2024**, *14*, 311. [CrossRef]
2. Sharma, S.; Palaniappan, K.; Mishra, V.D. Mechanical Characterization of Near-Isotropic Inconel 718 Fabricated by Laser Powder-Bed Fusion. *Metall. Mater. Trans. A* **2023**, *54*, 270–285. [CrossRef]
3. Du, J.; Cheng, W.; Sun, Y.; Ma, R.; Liu, H.; Song, X.; Yang, J.; Tan, C. The Effect of Precipitates on the Stress Rupture Properties of Laser Powder Bed Fusion Inconel 718 Alloy. *Coatings* **2023**, *13*, 2087. [CrossRef]
4. Panteleenko, F.I.; Maksarov, V.V.; Petrishin, G.V. Fast Magnetic Abrasive Finishing with Diffusionally Alloyed Powder. *Russ. Eng. Res.* **2023**, *43*, 470–473.
5. Mousa, S.M.; Hameed, A.S.; Ibrahim, A.F. Measurement from the residual stresses on magnetic abrasive finishing process by utilizing steel sheet 201. In *Multiscale and Multidisciplinary Modeling, Experiments and Design*; Springer: Berlin/Heidelberg, Germany, 2024. [CrossRef]

6. Maraboina, R.; Pasam, V.K. Enhancing Surface Integrity of Selective Laser Melted Al-Si Alloys through Ultrasonic Assisted Magnetic Abrasive Finishing utilizing SiC Abrasives. *Silicon* **2024**, *16*, 1183–1196. [CrossRef]
7. Zhou, Z.; Sun, X.; Yang, Y.; Fu, Y. A Study on Using Magnetic Abrasive Finishing with a 6-Axis Robot to Polish the Internal Surface Finishing of Curved Tubes. *Coatings* **2023**, *13*, 1179. [CrossRef]
8. Zhang, X.; Zhao, X.; Cheng, B. Finishing mechanism modelling on magnetic abrasive finishing behaviours with core-shell magnetic abrasive particles. *Int. J. Adv. Manuf. Technol.* **2023**, *129*, 573–585. [CrossRef]
9. Kumar, Y.; Singh, H. Development of Novel Low-Cost Sintered Magnetic Abrasive for Surface Finishing. In *Advances in Micro and Nano Manufacturing and Surface Engineering*; Bhattacharyya, B., Mathew, J., Saravanakumar, N., Rajeshkumar, G., Eds.; Lecture Notes in Mechanical Engineering; Springer: Singapore, 2022. [CrossRef]
10. Zhang, W. Dynamic Accumulation Mechanism of Magnetic Abrasive Particles on the Saw Wire Surface. *Trans. Electr. Electron. Mater.* **2022**, *23*, 535–543. [CrossRef]
11. Wang, Z.; Ding, Y.; Wang, P. Research of dry tribochemical mechanical polishing SiC with an innovation abrasive-catalytic abrasive cluster. *Int. J. Adv. Manuf. Technol.* **2024**, *131*, 2365–2376. [CrossRef]
12. Mosavat, M.; Rahimi, A. Numerical-experimental study on polishing of silicon wafer using magnetic abrasive finishing process. *Wear* **2019**, *424–425*, 143–150. [CrossRef]
13. Guo, J.; Feng, W.; Jia, H. Finishing of rectangular microfeatures by localized vibration-assisted magnetic abrasive polishing method. *J. Manuf. Process.* **2020**, *49*, 204–213. [CrossRef]
14. Heng, L.; Kim, J.; Tu, J. Fabrication of precision meso-scale diameter ZrO_2 ceramic bars using new magnetic pole designs in ultra-precision magnetic abrasive finishing. *Ceram. Int.* **2020**, *46*, 17335–17346. [CrossRef]
15. Babbar, A.; Prakash, C.; Singh, S. Application of hybrid nature-inspired algorithm: Single and bi-objective constrained optimization of magnetic abrasive finishing process parameters. *J. Mater. Res. Technol.* **2020**, *9*, 7961–7974. [CrossRef]
16. Tan, Y.; Ni, Y.; Xu, W. Key technologies and development trends of the soft abrasive flow finishing method. *J. Zhejiang Univ. Sci. A* **2023**, *24*, 1043–1064. [CrossRef]
17. Wang, Z.; Yang, Y.; Wang, S. The Effect of Hydrogen Peroxide on Composite Lapping of Titanium Alloy (TC4) by Free Abrasive Assisted Fixed Abrasive. *J. Inst. Eng. India Ser. E* **2023**, *104*, 171–183. [CrossRef]
18. Li, W.; Li, J.; Cheng, B. Achieving in-situ alloy-hardening core-shell structured carbonyl iron powders for magnetic abrasive finishing. *Mater. Des.* **2021**, *212*, 110198. [CrossRef]
19. Jiang, L.; Chang, T.; Zhang, G. Influence of process conditions on preparation of CBN/Fe-based spherical magnetic abrasive via gas atomization. *Ceram. Int.* **2021**, *47*, 31367–31374. [CrossRef]
20. Jiang, L.; Chang, T.; Zhang, G. Formation mechanism of ceramic/metal composite spherical magnetic abrasive prepared via gas-solid atomization. *J. Alloys Compd.* **2022**, *923*, 166400. [CrossRef]
21. Jiang, L.; Zhang, G.; Du, J. Processing performance of Al_2O_3/Fe-based composite spherical magnetic abrasive particles. *J. Magn. Magn. Mater.* **2021**, *528*, 167811. [CrossRef]